Operation and Design Principles of a PM Vernier Motor

Byungtaek Kim, *Member, IEEE*, and Thomas A. Lipo, *Life Fellow, IEEE*

***Abstract*—In this paper, the back electromotive force and power equations of a permanent-magnet (PM) vernier motor are accurately derived considering an air-gap permeance function expressed in terms of practical machine dimensions. Using these equations, the nature of a PM vernier motor is analytically surveyed, and substantial information such as main geometric factors affecting torque and the maximally obtainable torque for a given current are provided, leading to a new relation for torque per air-gap volume. In addition, these equations provide a means to determine the slot and pole combinations to realize greater power density. Finally, the effects of an increased reactance are investigated in respect to machine performance with a given voltage.**

***Index Terms*—Design principle, permanent-magnet machine, permeance function, vernier motor.**

I. Introduction

WHILE the vernier reluctance motor has a history dating back more than 50 years [1], the concept of a permanent-magnet (PM) vernier motor was first presented less than 20 years ago [2]. In those studies, however, it appears that the torque and power equations derived were exaggerated due to an ambiguous interpretation of the air-gap permeance. Therefore, there has been a substantial gap between the experimental and theoretical results as an outcome of this work [3]–[5].

For a long period afterward, studies on this machine topology essentially came to a halt. However, recently, magnetic gears with the same vernier principle have been actively researched [6]–[10], and several research studies on the vernier motor have been also presented [11]–[16]. However, most of them have focused on improving the power factor, which was pointed out as the main problem in previous studies [3]–[5], and to that aim, these authors proposed their own structures such as split-slot, fractional slots, and dual air gaps. However, because they still have used the previously developed power equation [2] with unclear air-gap permeance, their research results were limited in comparison with other machines, not providing equations considering details of the machine's practical design parameters.

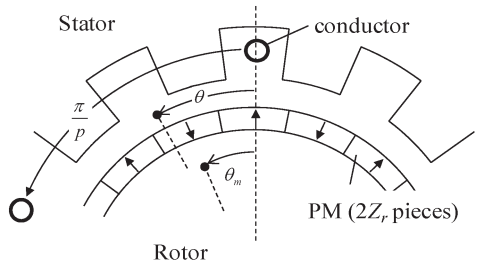

Fig. 1. Portion of PM vernier motor geometry.

In this paper, in order to reveal the nature of vernier machine more deeply, the general back electromotive force (EMF) equation, including machines' geometry instead of an ambiguous permeance function, is derived. To this aim, the permeance distribution in air gap, which is the underlying mechanism for developing torque in the vernier motor, is efficiently dealt with by using a harmonic series expressed in terms of practical machine's geometry. Therefore, the derived equation provides considerable information of the vernier machine useful for comparison to a conventional PM motor. Using this equation, the back EMF characteristics can be predicted taking into account many factors, including mechanical geometry and electrical specifications, and optimal combinations to realize greater power are given. These equations lead to a very new relation for torque per unit volume, which is quite different from a conventional machine. To prove its validity, a proto machine with a given diameter was selected, and various finite-element analyses (FEAs) have been performed and results are compared. Finally, the power factor problem due to high-frequency operation is discussed and clarified.

II. Derivation of Back EMF and Power Equation

A. Valid Combinations of Magnets and Slots

To develop the back EMF of a vernier motor, a portion of a surface PM motor shown in Fig. 1 is assumed. The MMF developed by PM $F_{\rm PM}$ and the specific air-gap permeance P are expressed by (1) and (2), respectively, where each of the coefficients is determined by geometries of the stator slots and magnets

$$F_{\rm PM}(\theta,\theta_m) \approx F_{\rm PM1}\cos\ Z_r(\theta-\theta_m) \tag{1}$$

$$P(\theta) \approx P_0 - P_1\cos(Z_s\theta) \tag{2}$$

Manuscript received October 11, 2013; revised January 22, 2014; accepted February 28, 2014. Date of publication March 25, 2014; date of current version November 18, 2014. Paper 2013-EMC-766.R1, presented at the 2013 IEEE Energy Conversion Congress and Exposition, Denver, CO, USA, September 16–20, and approved for publication in the IEEE Transactions on Industry Applications by the Electric Machines Committee of the IEEE Industry Applications Society. This work was supported by Kunsan National University's Long-term Overseas Research Program for Faculty Member in 2012.

B. Kim is with the Department of Electrical Engineering, Kunsan National University, Gunsan 573-701, Korea (e-mail: btkim@kunsan.ac.kr).

T. A. Lipo is with the Department of Electrical and Computer Engineering, University of Wisconsin-Madison, Madison, WI 53706-1691 USA (e-mail: lipo@engr.wisc.edu).

Color versions of one or more of the figures in this paper are available online at http://ieeexplore.ieee.org.

Digital Object Identifier 10.1109/TIA.2014.2313693

0093-9994 © 2014 IEEE. Personal use is permitted, but republication/redistribution requires IEEE permission.
See http://www.ieee.org/publications_standards/publications/rights/index.html for more information.

where Z_s is the stator slot number, and Z_r is the number of pairs of rotor magnets. Using (1) and (2), the air-gap flux density is given as

$$\begin{aligned} B(\theta,\theta_m) &= F_{\rm PM}(\theta,\theta_m)P(\theta) \\ &= B_{\rm PM0}\cos\ Z_r(\theta-\theta_m) - \frac{B_{\rm PM1}}{2} \\ &\quad\times\left(\cos\left((Z_r-Z_s)\theta - Z_r\theta_m\right)\right. \\ &\quad\left.+\cos\left((Z_r+Z_s)\theta - Z_r\theta_m\right)\right) \end{aligned} \tag{3}$$

where $B_{\rm PM0} = F_{\rm PM1}P_0$ and $B_{\rm PM1} = F_{\rm PM1}P_1$.

If p pole pairs, full pitch, and q slots/phase/pole are assumed for the stator winding, the stator flux linkage can be expressed as

$$\begin{aligned} \lambda_{\rm ph}(\theta_m) &= \frac{N_{\rm ph}r_g l_{\rm stk}}{q}\sum_{k=0}^{q-1}\int_{\theta_i+k\alpha_T}^{\theta_{\rm ph}+k\alpha_T+\pi/p} B(\theta,\theta_m)d\theta \\ &= \frac{N_{\rm ph}r_g l_{\rm stk}}{q}\sum_{k=0}^{q-1} \\ &\quad\times\left[\frac{B_{\rm PM0}}{Z_r}\sin\left(Z_r(\theta-\theta_m)\right) - \frac{B_{\rm PM1}}{2}\right. \\ &\quad\times\left\{\frac{\sin\left((Z_r-Z_s)\theta - Z_r\theta_m\right)}{(Z_r-Z_s)}\right. \\ &\quad\left.\left.+\frac{\sin\left((Z_r+Z_s)\theta - Z_r\theta_m\right)}{(Z_r+Z_s)}\right\}\right]_{\theta_{\rm ph}+k\alpha_T}^{\theta_{\rm ph}+k\alpha_T+\pi/p} \end{aligned} \tag{4}$$

where $N_{\rm ph}$ is the number of series turns per phase, r_g is the air-gap radius, $l_{\rm stk}$ is the stack length of core, $\alpha_T = 2\pi/Z_s = 2\pi/6pq$, and $\theta_{\rm ph}$ is the initial angular position of each phase winding assumed as 0, $2\pi/3$, and $4\pi/3$, respectively, for convenience.

Since $Z_r = p$ for a conventional PM machine, the second terms in the parentheses in (4) become negligible, and (4) is expressed by (5). When the rotor is rotating with the mechanical speed of $d\theta_m/dt = \omega_m$, the well-known back EMF in (6) is obtained, where k_{1q} is the fundamental component winding factor and D_g is the air-gap diameter

$$\begin{aligned} \lambda_{\rm ph}(\theta_m) &\approx \frac{N_{\rm ph}r_g l_{\rm stk}}{q}\frac{2B_{\rm PM0}}{p}\sum_{k=0}^{q-1}\sin\left(p\theta_m - p\theta_{\rm ph} - k\frac{\pi}{3q}\right) \\ &= k_{1q}N_{\rm ph}D_g l_{\rm stk}\frac{B_{\rm PM0}}{p}\sin\ p(\theta_m-\theta_{\rm ph}) \end{aligned} \tag{5}$$

$$e_{\rm ph}(t) = k_{1q}N_{\rm ph}D_g l_{\rm stk}\omega_m B_{\rm PM0}\cos\ p(\theta_m-\theta_{\rm ph}). \tag{6}$$

On the other hand, for a vernier motor, one must instead focus on the second term in (4), wherein $Z_r - Z_s = \pm p$ is chosen. In this case, the following flux linkage and back EMF equations

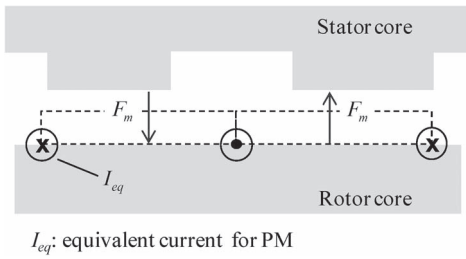

Fig. 2. Typical air-gap portion of the machine.

are obtained by using $Z_r = p(6q \pm 1)$, $\alpha_T = 2\pi/6pq$, and $6pq\theta_{\rm ph}$ equal to multiples of 2π:

$$\begin{aligned} e_{\rm ph}(t) &= \frac{d}{dt}\lambda_{\rm ph}(\theta_m) \\ &= \frac{d}{dt}\left\{k_{1q}N_{\rm ph}D_g l_{\rm stk}\left(\frac{B_{\rm PM0}}{Z_r} \mp \frac{B_{\rm PM1}}{2p}\right)\right. \\ &\qquad\left.\times\sin\left(Z_r\theta_m \mp p\theta_{\rm ph}\right)\right\} \\ &= k_{1q}N_{\rm ph}D_g l_{\rm stk}\omega_m\left(B_{\rm PM0} \mp \frac{Z_r}{2p}B_{\rm PM1}\right) \\ &\quad\times\cos\left(Z_r\theta_m \mp p\theta_{\rm ph}\right) \end{aligned} \tag{7}$$

where the upper negative and the lower positive conventions are for $Z_r - Z_s = +p$ and $Z_r - Z_s = -p$, respectively.

It is easily seen that the back EMF, i.e., (7), consists of two terms and that the first term is identical with that of the conventional PM motor, i.e., (6). Upon comparing the back EMF, i.e., (6), with the first term of (7), it is seen that the torque production of the two machines based on the fundamental component of magnet MMF is the same. In addition, the net back EMF of the vernier motor is the sum of both this term and an additional term, which suggests that the total EMF can be possibly greater than the EMF of a conventional PM motor. The second term in (7) is a unique component produced by the vernier structure, which has been already studied in previous work [3], [4]. It can be noted that it appears that the back EMF and thus motor torque can be theoretically increased without limit since the second term is proportional to the number of pairs of rotor magnets Z_r. However, this tendency is ultimately not possible because of the limitation on $B_{\rm PM1}$ in (7), which, in turn, depends upon the shape of the slots. In any case, to obtain the benefit of a vernier motor, both terms should be clearly summed in a positive manner, and the condition to this end must be chosen that $Z_r - Z_s = -p$ as opposed to the positive value of p selected in previous papers [2]–[5].

B. Air-Gap Permeance Function

A more revealing expression for the back EMF equation of a vernier motor is obtained by recalling that $B_{\rm PM0} = F_{\rm PM1}P_0$ and $B_{\rm PM1} = F_{\rm PM1}P_1$ in (1) and noting that $Z_r = 6pq - p$. When these terms are substituted in (7), one obtains

$$E_{\rm ph} = \frac{k_{1q}N_{\rm ph}DL\omega_m}{\sqrt{2}}\left\{F_{\rm PM1}\left(P_0 + \frac{6q-1}{2}P_1\right)\right\}. \tag{8}$$

Here, $F_{\rm PM1}$ is the fundamental component of MMF F_m, which is developed by the PM and for the case of Fig. 2. It

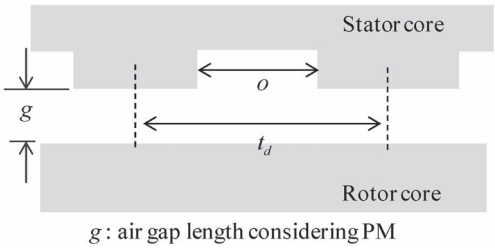

Fig. 3. Open-slot parameters.

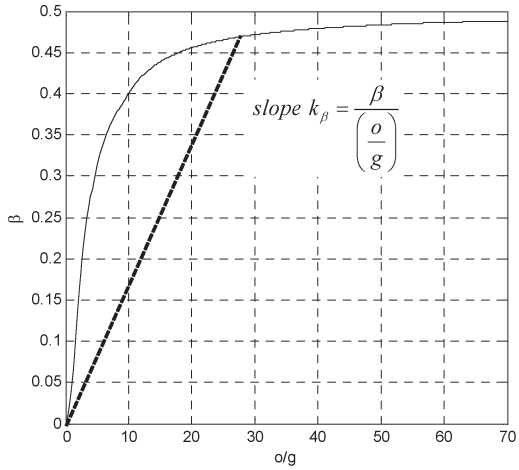

Fig. 4. Parameter β versus o/g.

is represented by

$$F_{\mathrm{PM1}} = \frac{4}{\pi}\frac{B_r g_m}{\mu_m} \tag{9}$$

where B_r and μ_m are the residual flux density and permeability of the magnet, respectively. The permeance coefficients in (2) are a function of slot geometries and can be expressed in classical form using the conformal mapping method [18]. The resulting values of P_0 and P_1 in Fig. 3 are given as (10) and (11), respectively, where c_0 is the ratio of slot opening to a slot pitch o/t_d and g is the air-gap length considering magnet thickness g_m given by $g_a + g_m/\mu_r$, where g_a is the mechanical air-gap length and μ_r is the recoil permeability of magnet

$$P_0 = \frac{\mu_0}{g}(1 - 1.6\beta c_0) \tag{10}$$

$$P_1 = \frac{\mu_0}{g}\frac{2\beta}{\pi}\left(\frac{0.78}{0.78 - 2c_0^2}\right)\sin(1.6\pi c_0). \tag{11}$$

The quantity P_0 is an average air-gap permeance, which is actually an alternative form of the so-called Carter's coefficient. In (10) and (11), β is the nonlinear function of o/g shown in Fig. 4. It shows quite linear properties until o/g is less than 10 and then converges to 0.5 as o/g increases to infinity. Since the slot opening $o = c_0\pi D/Z_s = c_0\pi D/6pq$, β can be alternatively expressed as

$$\beta = k_\beta\frac{o}{g} = k_\beta c_o\frac{\pi D_g}{6pq}\frac{1}{g} \tag{12}$$

where coefficient k_β is the slope of the function β in Fig. 3. Using (10) and (11), accurate values of P_0 and P_1 can be obtained for a given structure.

C. Back EMF Characteristics

Using (9)–(11), the back EMF in (8) can be replaced by the following:

$$E_{\mathrm{ph}} = \frac{2\sqrt{2}B_r}{\pi\mu_r}k_{1q}N_{\mathrm{ph}}D_g l_{\mathrm{stk}}\omega_m\frac{g_m}{g}(K_{\mathrm{conv}} + K_{\mathrm{add}}) \tag{13}$$

where K_{conv} is for the coefficient for a conventional motor, and K_{add} is for the additional term for a vernier motor, which are expressed by (13) and (14)

$$K_{\mathrm{conv}} = 1 - 1.6k_\beta\frac{\pi D_g}{6pqg}c_0^2 \tag{14}$$

$$K_{\mathrm{add}} = k_\beta c_o\frac{\pi D_g}{pg}\left(1 - \frac{1}{6q}\right)\left(\frac{0.78}{0.78 - 2c_0^2}\right) \times \sin(1.6\pi c_o). \tag{15}$$

The negative second term in (14) reflects an increase in effective air-gap length due to slot opening and has a relatively small value in practice. In (15), it is easily seen that the variables affecting K_{add} are c_0, D/g, q, and p and that p should be small as possible to obtain a high back EMF in the linear area of k_β. Using (14) and (15), K_{conv} and K_{add} can be obtained, and for a vernier motor with $D_g = 400$ mm and $g_a = 3$ mm, their characteristics are investigated with various values of c_0, q, and g_m. Fig. 5 shows their characteristics with c_0 and g_m when $q = 2$. Fig. 5(a) represents the fact that as c_0 becomes greater, K_{conv} becomes smaller because the effective air-gap length becomes larger. K_{conv} also increases with g_m, which is natural for a conventional motor.

However, K_{add} in Fig. 5(b) clearly illustrates the different design characteristics of a vernier motor. Unlike a conventional motor, this quantity reaches a maximum at specific magnet thickness and then keeps decreasing, although the magnet thickness increases, because of the decreasing value of P_1 in (11). For most cases, K_{add} maximizes around $c_0 = 0.5{-}0.6$, the ratio of slot open to slot pitch, which is easily explained by calculating $\partial P_1/\partial c_0 = 0$.

The sum of K_{conv} and K_{add}, K_{ver} is represented in Fig. 4(c) showing that the maximum back EMF can reach up to almost two times $(K_{\mathrm{ver}}/K_{\mathrm{conv}})$ that of a conventional PM motor at $g_m = 8$ mm and $c_0 = 0.6$ for the given case $(q = 2)$.

With $c_0 = 0.6$, since it is known that K_{ver} is maximized around this value, characteristics for various values of q can be investigated and are shown in Fig. 5. For fair comparison with a conventional machine, c_0 of a conventional machine is set to 0.1 and $q = 1$ to obtain greater back EMF. In Fig. 6, it is shown that K_{ver} converges to a specific value with the increase in q, which is easily explained and calculated by (15). This result clears up the ambiguity of power or back EMF in previous studies in which it appears to keep increasing with q, consequently increasing $Z_r = p(6q - 1)$ in (7). Therefore, it should be noticed that while q increases (which means that Z_r increases), K_{add} is not greatly affected, particularly when q is greater than 2. This result clearly shows that the design values of conventional machine designs are well suited for a practical vernier motor. The maximum value of K_{ver} reaches above 2.5 when q continues to increase.

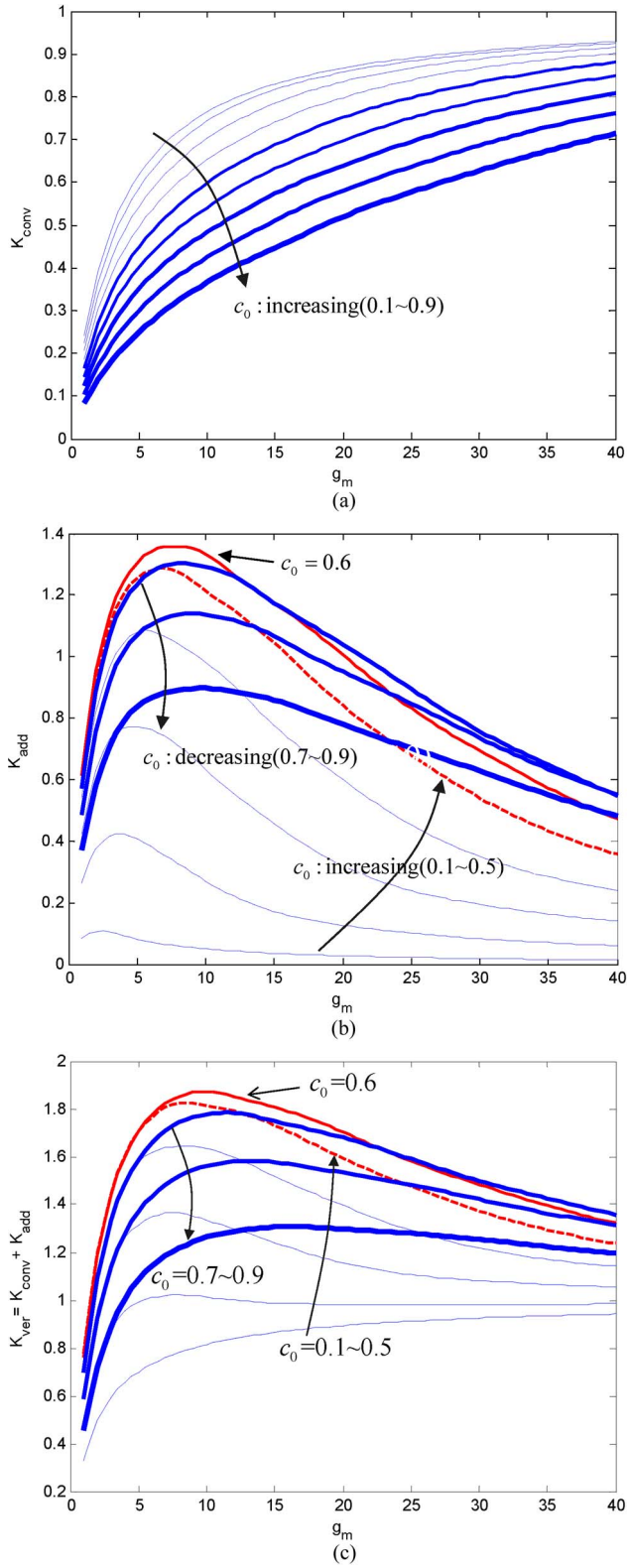

Fig. 5. Variation of $K_{\rm conv}$, $K_{\rm add}$, and $K_{\rm ver}$ with c_0 and g_m (a) $K_{\rm conv}$. (b) $K_{\rm add}$. (c) $K_{\rm ver}$.

D. Characteristic of Power Per Air-Gap Volume

Since the mechanical power of the PM machine is the product of current and back EMFs and the winding current is normally limited by surface current density K_s, the power is alternatively expressed as

$$\begin{aligned} P_o &= 3I_{\rm ph}E_{\rm ph} \\ &= \frac{\sqrt{2}B_r}{\mu_r}k_{1q}K_s D_g^2 l_{\rm stk}\omega_m \frac{g_m}{g}(K_{\rm conv}+K_{\rm add}) \\ &= K_\tau \omega_m V_g \frac{g_m}{g}(K_{\rm conv}+K_{\rm add}) \end{aligned} \tag{16}$$

where $K_s = (6N_{\rm ph}I_{\rm ph}/\pi D_g)$, $K_\tau = (4\sqrt{2}B_r/\pi\mu_r)k_{1q}K_s$, and V_g is the air-gap volume.

For a machine with given c_0, p, and q and dealing with them as constant k_o, (16) simplifies to

$$P_o = K_\tau \omega_m V_g \frac{g_m}{g}\left(1 + k_o k_\beta \frac{D_g}{g}\right). \tag{17}$$

This equation obviously shows the benefits of vernier motor with respect to the machine's air-gap volume necessary for a given power. In the parentheses of (17), the first term represents the well-known proportional relation between the air-gap volume and power, but due to the second term, as the diameter increases with a fixed gap length, the volume for a given power decreases. From this equation, it can be expected that the vernier motor will be very suitable for a machine with a larger diameter.

The effects of D_g/g in (17) were investigated by decreasing g instead of D_g. Since g consists of the air-gap length and magnet thickness in this structure, $K_{\rm ver}$ for various air-gap lengths are calculated and compared with $K_{\rm conv}$ (with $c_0 = 0.1$ and $q = 2$) in Fig. 7. From the results, it can be seen that the gap length also increases the maximum back EMF substantially, which is almost three times that of a conventional motor, which also means that back EMF or power with the same current is three times that of a conventional motor.

The above results from the back EMF equation are summarized as follows. It should be apparent now that the vernier motor has a greater back EMF and power density than a conventional PM machine. The back EMF mainly depends on

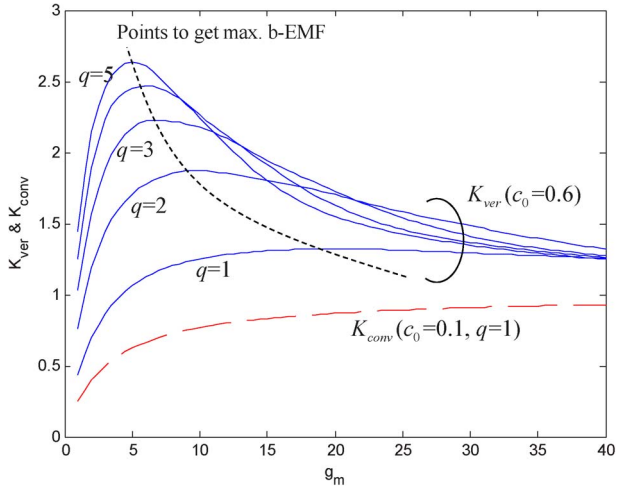

Fig. 6. Variation of $K_{\rm ver}$ and $K_{\rm conv}$ with q and g_m.

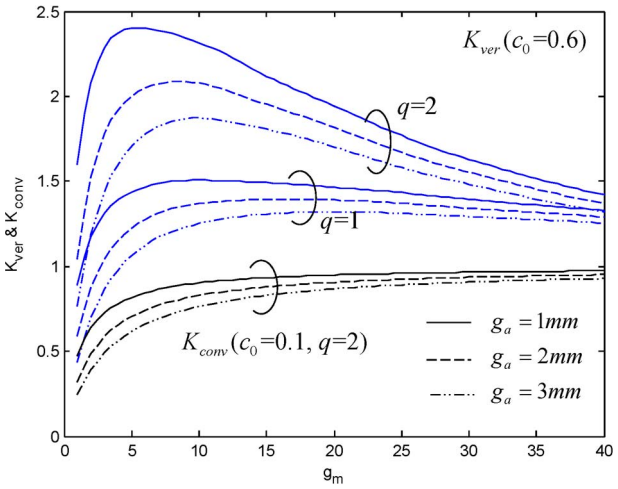

Fig. 7. Variation of $K_{\rm ver}$ and $K_{\rm conv}$ with g_a and g_m.

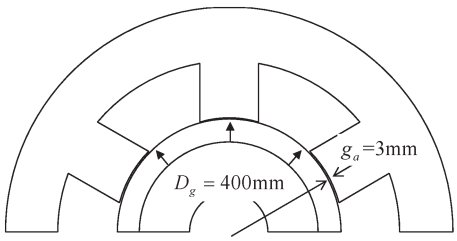

Fig. 8. Sample motor prototype.

c_0, q, g_m, and D_g/g. The best value of c_0 is around 0.5–0.6. As q increases, back EMF becomes somewhat greater, but its effects tend to be negligible when q is above 3. D_g/g is the most effective factor to increase the back EMF. As D_g/g becomes greater, the back EMF substantially increases, which also means that the use of a thin magnet is better for obtaining a higher back EMF in a vernier motor contrary to that of a conventional motor.

III. Back EMF Verification With Finite-Element Method

To verify the derived equations and results in Fig. 7, a simple PM motor with one pole pair p, 2-mm air gap g_a, and 400-mm air-gap diameter D_g is used for analysis. Fig. 8 shows the rough dimension in the case of $q = 1$. For convenience, it is assumed that the total number of series turns $N_{\rm ph}$ is 2, and the stack length $l_{\rm stk}$ is 250 mm. The magnet is assumed to be NdFeB with 1.1 T of residual flux density. To remove extra effects on the back EMF, the finite-element (FE) simulations were performed without considering eddy currents in magnets and ferromagnetic cores, but nonlinear B–H characteristics of core were taken into account.

While c_0 is fixed to 0.6, three kinds of stators for vernier and conventional motors have been modeled for FEA, as shown in Fig. 9. Each rotor with different pole pairs for stator was modeled with various magnet thicknesses.

Flux lines for each motor at a given moment are depicted in Fig. 10. It is shown that vernier motors have more magnets compared with the conventional motor, and their flux lines

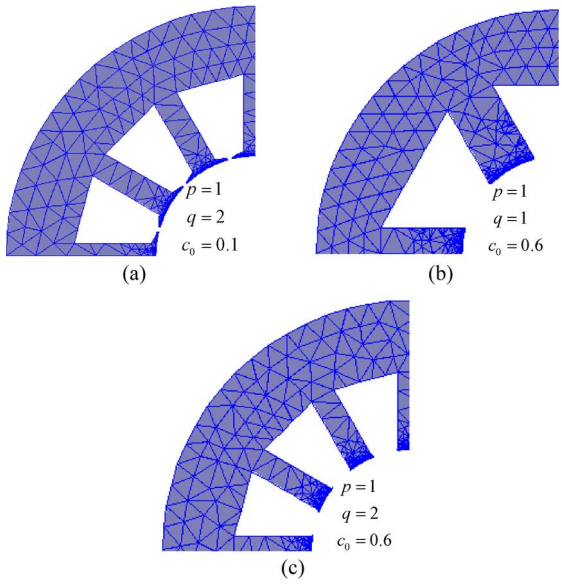

Fig. 9. FE modeled stators. (a) For conventional $(q = 2)$. (b) For vernier $(q = 1)$. (c) For vernier $(q = 2)$.

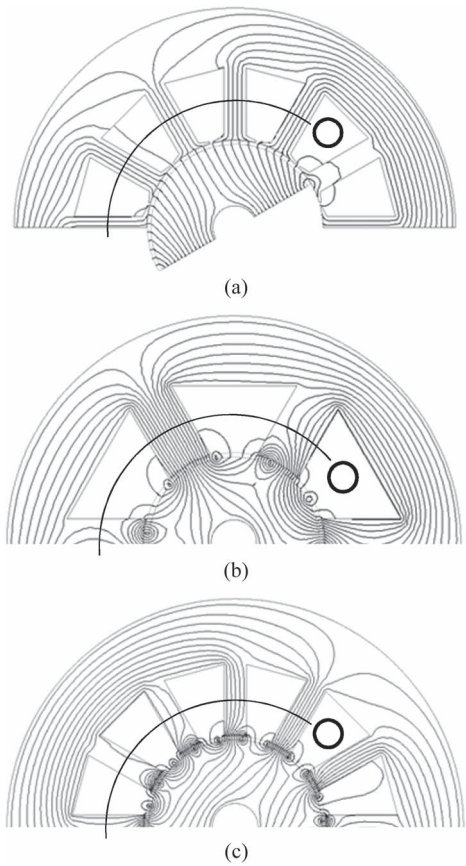

Fig. 10. Potential lines of conventional and vernier PM motors (one coil and its span are sketched). (a) Conventional $(q = 2)$. (b) Vernier $(q = 1)$. (c) Vernier $(q = 2)$.

pass between magnet pieces, not all linking stator windings. However, it should be reminded that these lines do not represent the leakage flux of the PM but consist of the quantity $B_{\rm PM0}$ in (3). In Fig. 10(b) and (c), the poles produced by $B_{\rm PM1}$ also can be easily found.

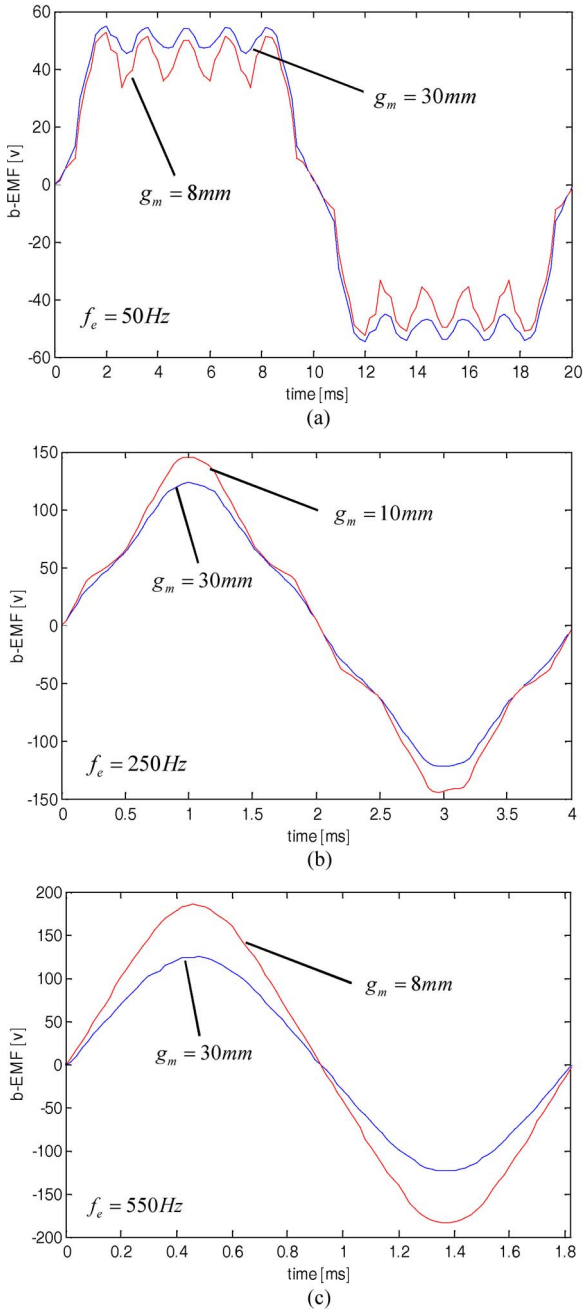

Fig. 11. Back EMF waveforms for various stators. (a) Conventional ($q = 2$). (b) Vernier ($q = 1$). (c) Vernier ($q = 2$).

The back EMFs were calculated for the case where the rotor rotates with 3000 r/min, and one-period waveforms are represented in Fig. 11. It should be noted that each period T is different with each other depending upon the number of magnets on the rotor. Fig. 11(a) shows the back EMF waveforms of a conventional motor with one pair of magnets, which are roughly 50 V regardless of magnet thickness that coincides well with the results in Fig. 7. On the other hand, the back EMFs of a vernier motor with $q = 1$ are shown in Fig. 11(b). It is shown that the voltages are around 120–140 V much larger than 50 V of conventional motors and the voltage becomes slightly higher although the magnet becomes thinner, i.e., 10 mm from 30 mm. Finally, Fig. 11(c) shows the back EMF of a vernier motor

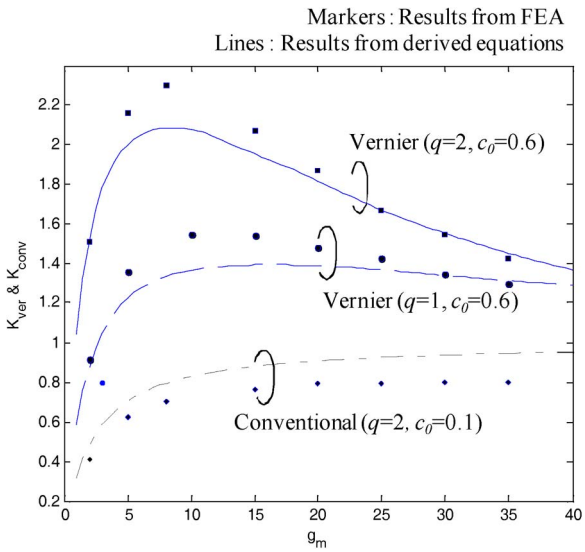

Fig. 12. Comparison of analytic and FE results.

with $q = 2$. It is clearly seen that the back EMF is dramatically increased in the vernier motor in spite of having less magnet thickness, as predicted in Figs. 5 and 7.

By using (13) and the additionally obtained back EMF results of FEA and Fig. 11, $K_{\rm conv}$ and $K_{\rm ver}$ can be obtained and compared with the analytic results in Fig. 12. It shows that the results coincide very well with each other, guaranteeing that the derived equations are sufficiently accurate to show the characteristics of the vernier motor. The results also suggest that two to three times mechanical torque can be obtained with an identical stator, including winding copper and identical current to a conventional PM motor. This result also means the same copper losses so that much higher efficiency is possible.

IV. Discussion of Power Factor

Thus far, the discussion has focused only on the back EMF of the vernier motor, and from the simulation results, it has been concluded that a vernier PM motor has much more power density than a conventional PM motor with the same volume. This conclusion is apparently true provided that the same current flows in the same winding. However, the motor is generally driven by a voltage source; hence, it is necessary to estimate the capacity of the voltage source to drive such a current, which is directly related with the power factor. In practice, many previous studies considered the poor power factor as a major problem of a vernier motor and that it is caused by a large amount of leakage flux from magnet. This idea would be reasonable provided that the back EMF is greatly reduced by leakage flux. However, in this paper, the equations derived without considering the flux leakage show very close correlation with actual back EMF characteristics, which means that the previous explanation is not proper. Therefore, it is more reasonable to take the view that the impedance inherently overtakes the back EMF in a surface PM vernier structure. This paper has investigated the fundamental reason of poor power factor and estimates its value.

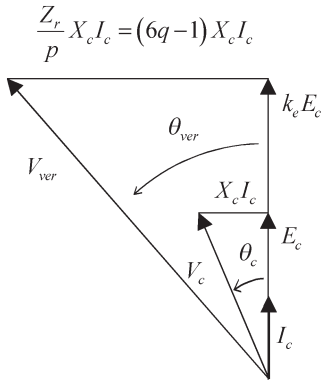

Fig. 13. Comparison of phasor diagrams.

In general, a vernier motor has a high operating frequency, as shown in Fig. 11, due to the use of more magnets on the rotor than a conventional machine. It also clearly causes the reactance to be much greater. On the other hand, the stator structure of a vernier motor is same as that of a conventional PM motor; thus, it has also the same winding inductance. However, the reactance becomes much greater because it is proportional to the operating frequency. Assume, for example, a stator with a conventional PM rotor that has back EMF E_c and reactance X_c and is driven by voltage V_c delivering a current I_c in phase with E_c. Neglecting the stator winding resistance, the phasor diagram can be drawn in Fig. 13, and the voltage is given by

$$V_c = \sqrt{E_c^2 + (X_c I_c)^2}. \tag{18}$$

If the same stator is operated as a vernier motor with a rotor having $2Z_r$ PMs, it can be assumed that the back EMF $k_e E_c$ and a reactance $Z_r X_c$ exist. Here, $Z_r = p(6q-1)$, and k_e is the coefficient of voltage boost, i.e., $K_{\rm ver}/K_{\rm conv}$. In this case, the required voltage $V_{\rm ver}$ to deliver the same current I_c is given by

$$V_{\rm ver} = \sqrt{k_e^2 E_c^2 + \left(\frac{Z_r}{p}\right)^2 (X_c I_c)^2}. \tag{19}$$

If k_e of the vernier motor is 1.5–3 in Figs. 4 and 5, Z_r becomes substantially greater than k_e when q is above 2 ($Z_r = 11$). Thus, from (18), $V_{\rm ver}$ will be substantially higher, thus aggravating the power factor, as shown in Fig. 13. The power factor of a vernier motor is expressed as (20), where angles $\theta_{\rm ver}$ and θ_c are the power angles of both in Fig. 13

$$\cos\theta_{\rm ver} = \frac{1}{\sqrt{1 + \left(\frac{Z_r}{pk_e}\right)^2 \tan^2\theta_c}}. \tag{20}$$

Using the results in Fig. 11, for instance, the power factors of a vernier motor were examined, which has originally 0.95 of power factor with conventional PM rotor, and are shown in Fig. 14. The result shows that as q increases, the power factor severely decreases. In particular, it is lower than 0.75 when $q = 2$ and $g_m = 10$ mm although the EMF is maximized than when $q = 1$. This result means that inverter capacity must increase substantially. Therefore, to design a surface PM vernier motor, in conclusion, it is generally desirable to choose the slots per pole per phase q to be lower than 3.

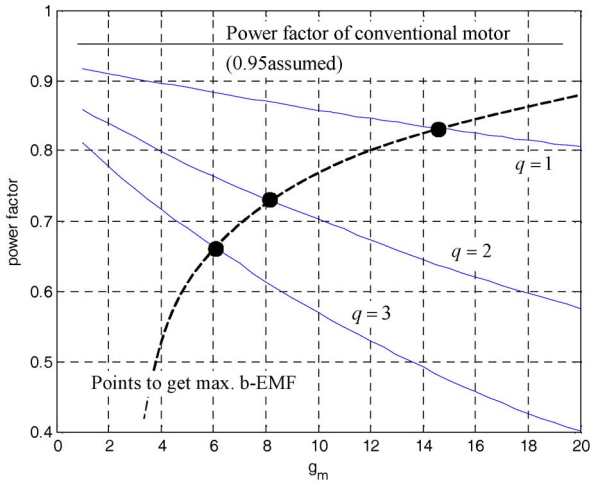

Fig. 14. Variation of power factor with q and g_m.

V. Conclusion

This paper has presented an analytically derived back EMF equation of a vernier motor using the classical permeance function. Using the obtained equation, the maximum achievable back EMF and power density of a vernier motor have been calculated analytically. To check the results, a FEA has been performed for a simply devised model and the usefulness is proven. To consider the voltage-driven situation, the power factor characteristics have been also examined according to various cases. From the results, the following have been determined.

First, in a vernier motor, the back EMF of a conventional PM motor, as well as an additional back EMF by first harmonic of air-gap permeance, was developed. The condition to sum the two terms in a positive manner is $Z_r - Z_s = -p$. Second, the geometric variables greatly affecting additional back EMF are the ratio slot opening width and pitch and the ratio of air-gap diameter and effective air-gap length. Unlike previous studies, it is shown that the effects of slot number become very limited as the number increases. Third, from the simulation results, two to three times back EMF and torque of a conventional PM motor appear possible to be obtained from a vernier motor with the same volume. From the derived relation of power and air-gap volume, the power density of the vernier motor becomes larger as air-gap diameter increases. Finally, to force the current to flow in a vernier motor, an excessive voltage may be necessary when q is greater than 2. These observations suggest that for optimum use of this type of machine, it is desirable that new structures with low inductance be developed in the future.

References

[1] C. H. Lee, "Vernier motor and its design," *IEEE Trans. Power App. Syst.*, vol. PAS-82, no. 66, pp. 343–349, Jun. 1960.

[2] A. Ishizaki, T. Tanaka, K. Takahashi, and S. Nishikata, "Theory and optimum design of PM Vernier motor," in *Proc. ICEMD*, 1995, pp. 208–212.

[3] A. Toba and T. A. Lipo, "Novel dual-excitation permanent magnet Vernier machine," in *Conf. Rec. IEEE 34th IAS Annu. Meeting*, 1999, pp. 2539–2544.
[4] A. Toba and T. A. Lipo, "Generic torque-maximizing design methodology of surface permanent-magnet Vernier machine," *IEEE Trans. Ind. Appl.*, vol. 36, no. 6, pp. 1539–1546, Nov./Dec. 2000.
[5] A. Toba and T. A. Lipo, "Experimental evaluations of the dual-excitation permanent magnet Vernier machine," presented at the Conf. Int. Power Electronics, Tokyo, Japan, Apr. 3–7, 2001, Paper S-22-3.
[6] K. Tsurumoto and S. Kikuchi, "A new magnetic gear using permanent magnet," *IEEE Trans. Magn.*, vol. 23, no. 5, pp. 3622–3624, Sep. 1987.
[7] K. Atallah, S. D. Calverley, and D. Howe, "Design, analysis and realisation of a high-performance magnetic gear," *Proc. Inst. Elect. Eng.—Elect. Power Appl.*, vol. 151, no. 2, pp. 135–143, Mar. 2004.
[8] P. O. Rasmussen, T. O. Andersen, F. T. Jorgensen, and O. Nielsen, "Development of a high-performance magnetic gear," *IEEE Trans. Ind. Appl.*, vol. 41, no. 3, pp. 764–777, May/Jun. 2005.
[9] K. T. Chau, D. Zhang, J. Z. Jiang, C. Liu, and Y. Zhang, "Design of a magnetic-geared outer-rotor permanent-magnet brushless motor for electric vehicles," *IEEE Trans. Magn.*, vol. 43, no. 6, pp. 2504–2506, Jun. 2007.
[10] D. J. Evans and Z. Q. Zhu, "Influence of design parameters on magnetic gear's torque capability," in *Proc. IEEE IEMDC*, 2011, pp. 1403–1408.
[11] R. Qu, D. Li, and J. Wang, "Relationship between magnetic gears and vernier machines," in *Proc. ICEMS*, 2011, pp. 1–6.
[12] J. Li, D. Wu, X. Zhang, and S. Gao, "A new permanent magnet Vernier in-wheel motor for electric vehicles," in *Proc. IEEE VPCC*, 2010, pp. 1–6.
[13] S. L. Ho, S. Niu, and W. N. Fu, "Design and comparison of Vernier permanent magnet machines," *IEEE Trans. Magn.*, vol. 47, no. 10, pp. 3280–3283, Oct. 2011.
[14] S. Niu, S. L. Ho, and W. N. Fu, "A novel direct-drive dual-structure permanent magnet machine," *IEEE Trans. Magn.*, vol. 46, no. 6, pp. 2036–2039, Jun. 2010.
[15] H. Kakihata, Y. Katoka, and M. Takayma, "Design of surface permanent magnet-type Vernier motor," in *Proc. 15th Int. Conf. Elect. Mach. Syst.*, 2012, pp. 1–6.
[16] D. Li and R. Qu, "Sinusoidal back-EMF of Vernier permanent magnet machines," in *Proc. 15th Int. Conf. Elect. Mach. Syst.*, 2012, pp. 1–6.
[17] K. Okada, N. Niguchi, and K. Hirata, "Analysis of a Vernier motor with concentrated windings," *IEEE Trans. Magn.*, vol. 49, no. 5, pp. 2241–2244, May 2013.
[18] B. Heller and V. Hamata, *Harmonic Field Effects in Induction Machines*. Amsterdam, The Netherlands: Elsevier, 1977, pp. 54–67.

Byungtaek Kim (M'01) is a native of Seoul, Korea. He received the B.S., M.S., and Ph.D. degrees from Hanyang University, Seoul, in 1994, 1996, and 2001, respectively, all in electrical engineering.

He was with Samsung Electro-Mechanics, Inc. for seven years and LG Electronics, Inc. for three years. He became a Professor of electrical engineering with Kunsan National University, Gunsan, Korea, in 2005. In 2012, he was a Visiting Scholar with the Department of Electrical and Computer Engineering, University of Wisconsin-Madison, Madison, WI, USA. His research interests include electric machines and power electronics.

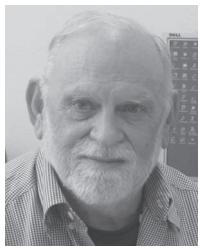

Thomas A. Lipo (M'64–SM'71–F'87–LF'00) is a native of Milwaukee, WI, USA.

From 1969 to 1979, he was an Electrical Engineer with the Power Electronics Laboratory, Corporate Research and Development, General Electric Company, Schenectady, NY, USA. He became a Professor of electrical engineering with Purdue University, West Lafayette, IN, USA, in 1979, and in 1981, he joined the University of Wisconsin-Madison, Madison, WI, USA, where he served as the W. W. Grainger Professor for Power Electronics and Electrical Machines for 28 years. He is currently an Emeritus Professor with the University of Wisconsin-Madison.

Prof. Lipo was elected a member of the Royal Academy of Engineering, London, U.K., in 2002; a member of the National Academy of Engineering, Washington, DC, USA, in 2008; and a member of the National Academy of Inventors, Tampa, FL, USA, in 2013. In 2014, he was selected to receive the IEEE Medal for Power Engineering. For the past 40 years, he has served the IEEE in numerous capacities, including President of the IEEE Industry Applications Society in 1994. He was the recipient of the Outstanding Achievement Award from the IEEE Industry Applications Society, the William E. Newell Award from the IEEE Power Electronics Society, and the 1995 Nicola Tesla IEEE Field Award from the IEEE Power Engineering Society for his work.